Supplementary Information

Self-driven microstructural evolution of Au@Pd core–shell nanoparticles for greatly enhanced catalytic performance during methanol electrooxidation

Yaxing Liu[a,b*], Weiyin Li[c], Guizhe Zhao[a,b], Gang Qin[d], Yuexia Li[b] and Yaqing Liu[a,b*]

[a] Shanxi Key Laboratory of Nano Functional Composite Materials, North University of China, Taiyuan, 030051, P. R. China

[b] School of Materials Science and Engineering, North University of China, Taiyuan, 030051, P. R. China

[c] School of Electrical and Information Engineering, North Minzu University, Yinchuan, 750021, P. R. China

[d] School of Materials Science and Engineering, Henan Polytechnic University, Jiaozuo, 454003, P. R. China

***Corresponding author:**

Yaxing Liu

Shanxi Key Laboratory of Nano Functional Composite Materials, School of Materials Science and Engineering, North University of China, Taiyuan, 030051, P. R. China

Email: yaxingliu@nuc.edu.cn

Yaqing Liu

Shanxi Key Laboratory of Nano Functional Composite Materials, School of Materials Science and Engineering, North University of China, Taiyuan, 030051, P. R. China

Email: lyq@nuc.edu.cn

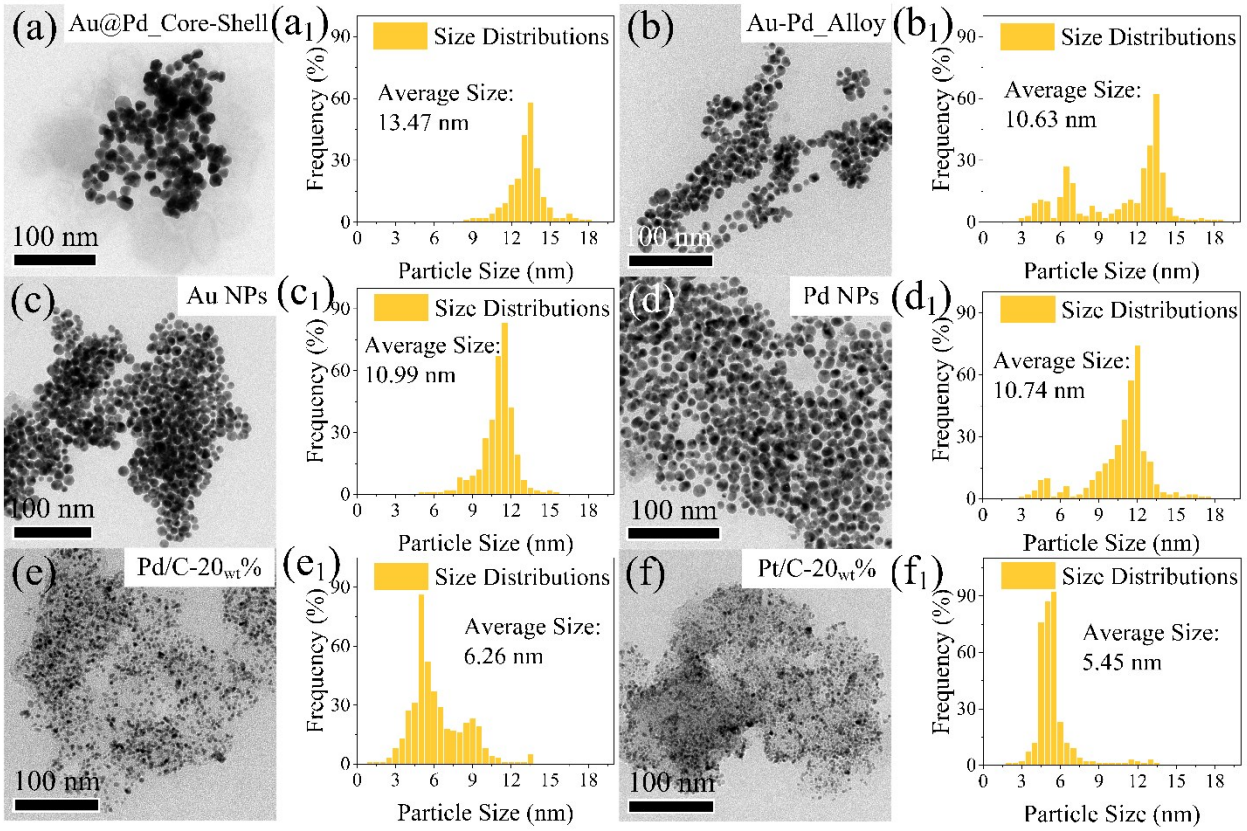

Figure S1 Bright field TEM images and corresponding nanoparticle size distributions of the as-prepared Au@Pd_Core-Shell (a, a_1), Au–Pd_Alloy (b, b_1), Au nanoparticles (c, c_1), Pd nanoparticles (d, d_1), Pd/C-20$_{wt}$% (e, e_1), and Pt/C-20$_{wt}$% (f, f_1).

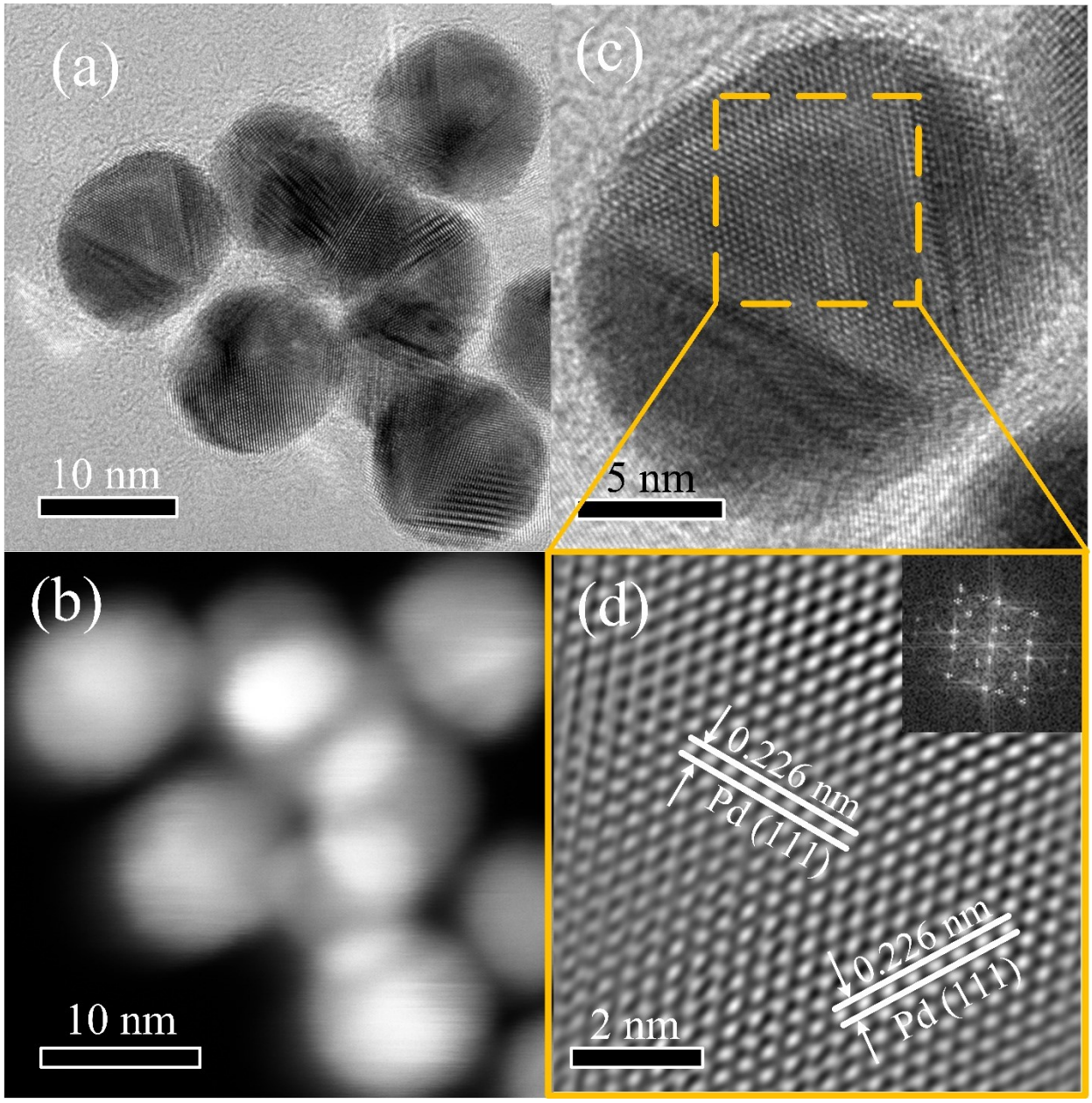

Figure S2 Microstructural characterization of the as-synthesized Pd NPs: (a) Bright and (b) dark field TEM images; (c) HR–TEM images; (d) selected-area inverse fast Fourier transform (IFFT) pattern of the region enclosed by the square in (c).

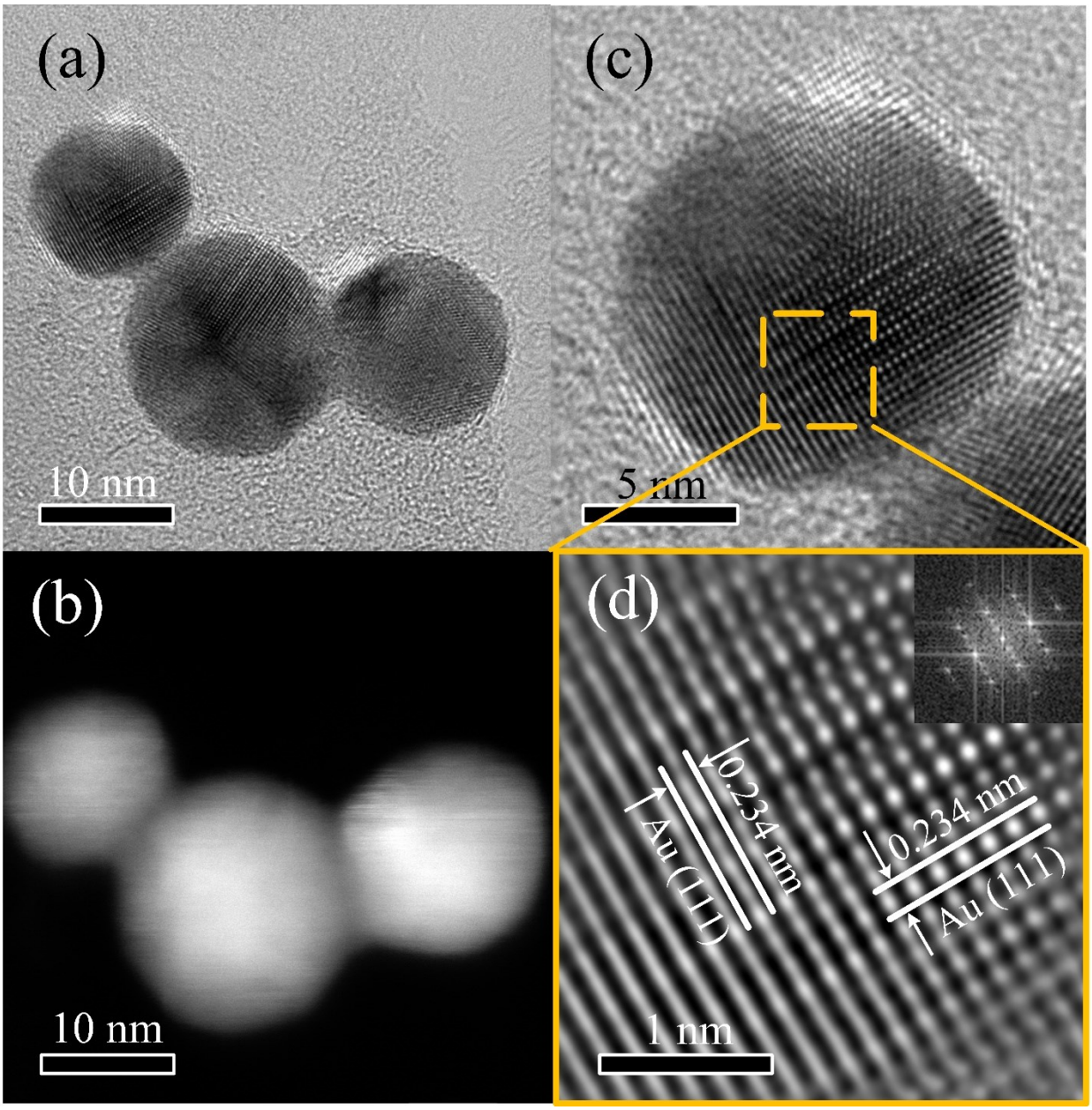

Figure S3 Microstructural characterization of the as-synthesized Au NPs: (a) Bright and (b) dark field TEM images; (c) HR–TEM image; (d) selected-area IFFT pattern of the region enclosed by the square in (c).

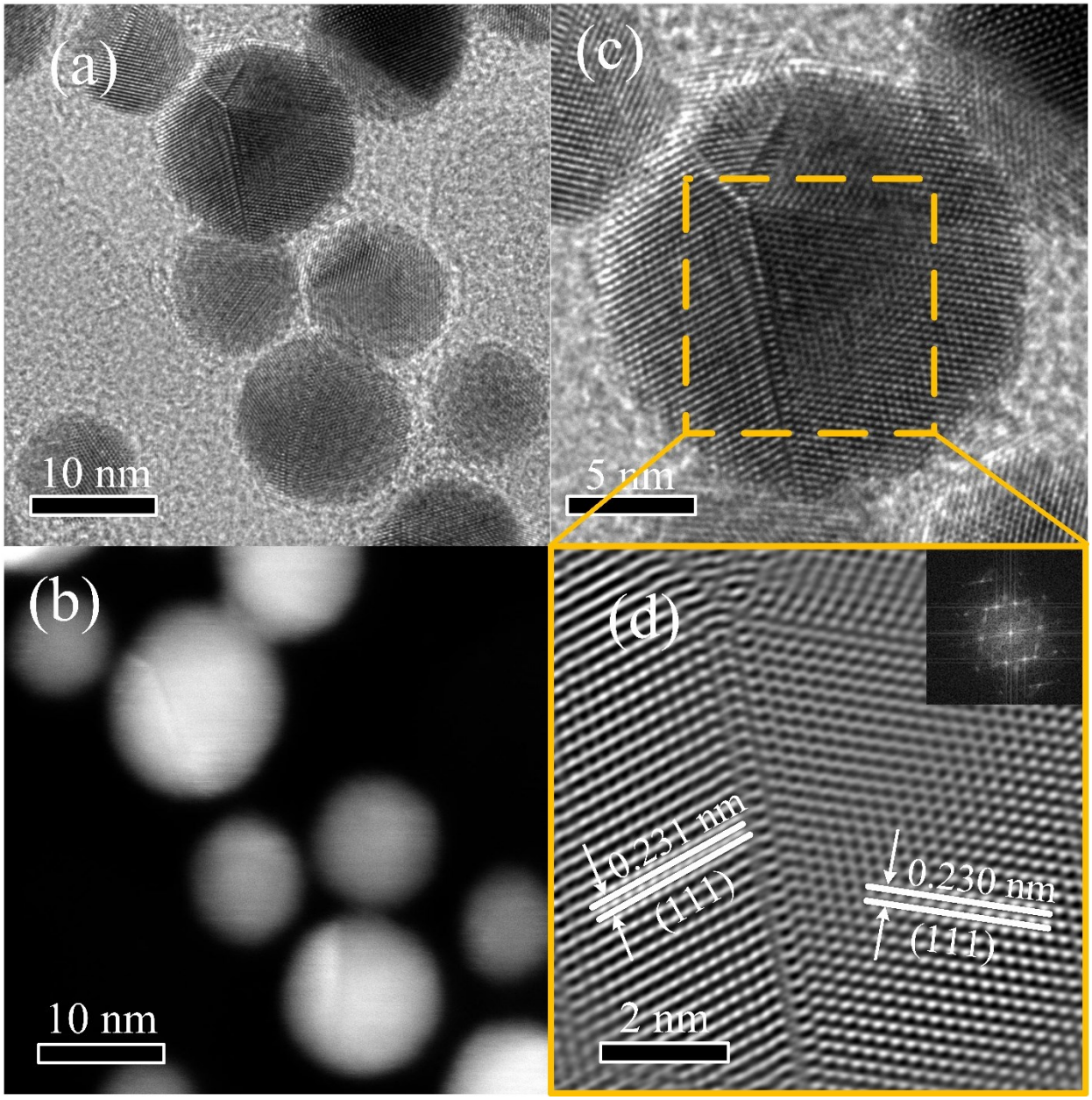

Figure S4 Microstructure characterization of the as-synthesized Au–Pd_Alloy nanoparticles: (a) Bright and (b) dark field TEM images; (c) HR–TEM image; (d) selected-area IFFT pattern enclosed by the square in (c).

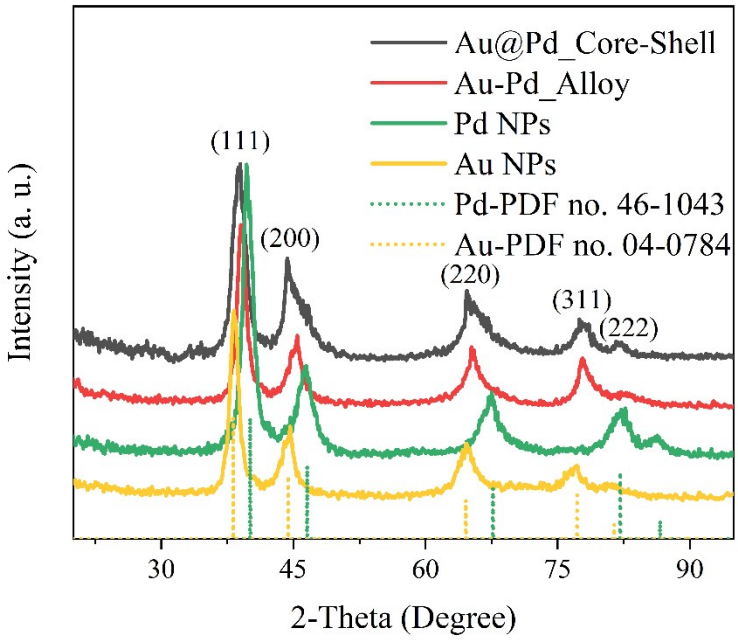

Figure S5 Comparisons of X-ray diffraction (XRD) patterns of the as-prepared Au@Pd_Core-Shell nanoparticles, Au–Pd_Alloy, Au nanoparticles, and Pd nanoparticles. The insets present the details of the corresponding diffraction peaks. Bar diagrams: Pd #46-1043 and Au #04-0784.

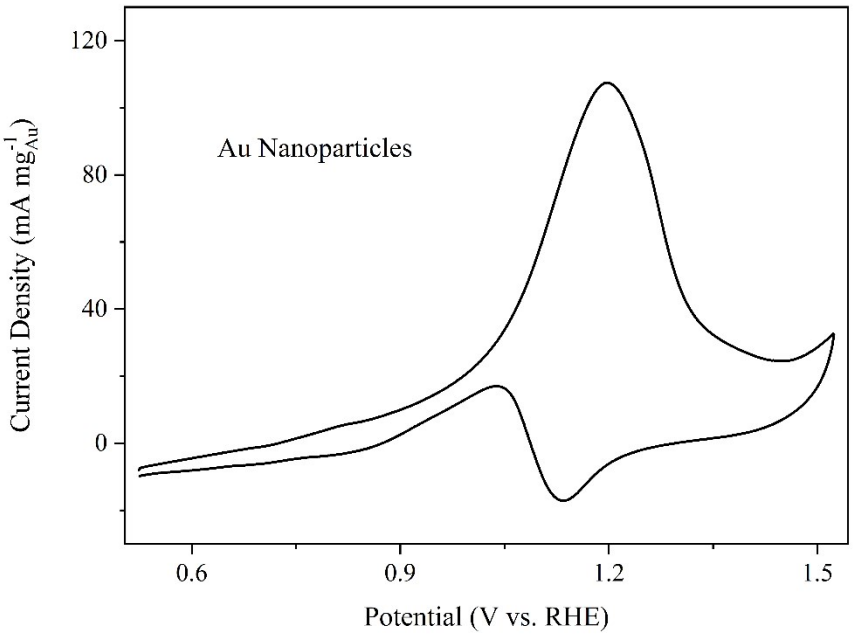

Figure S6 Methanol electrooxidation performances of the as-synthesized Au NPs. The CV curves were recorded in an N_2-saturated 1.0 M KOH solution with 1.0 M CH_3OH. The scan rate was 50 mV s^{-1}.

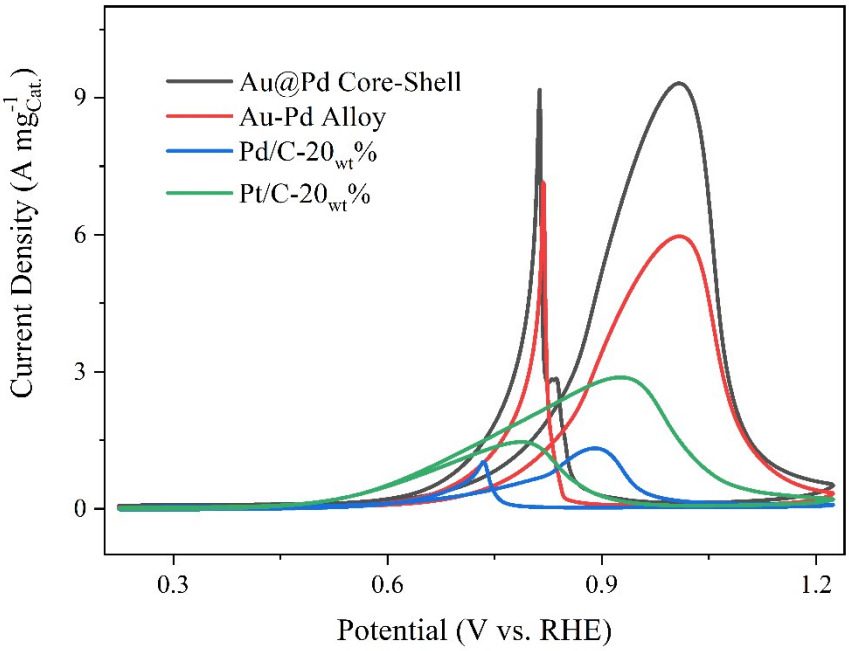

Figure S7 Methanol electrooxidation performances of the as-prepared Au@Pd_Core-Shell nanoparticles, Au–Pd_Alloy, commercial Pd/C-20$_{wt}$%, and commercial Pt/C-20$_{wt}$% catalysts. The CV curves were recorded in N_2-saturated 1.0 M KOH solution with 1.0 M CH_3OH. The scan rate was 50 mV s^{-1}.

Table S1 Comparison of mass activities of Pd-based electrocatalysts reported in the literature.

Sample	Current Density	Electrolyte	References
Au@Au-Pd_Core-Shell	9.35 (A mg−1 Cat.)	1.0 M KOH + 1.0 M CH_3OH	**This work**
Au@Au-Pd_Core-Shell	10.9 (mA cm^{-2})	1.0 M KOH + 1.0 M CH_3OH	**This work**
$Pd_{41}Au_{59}$	6.52 (mA cm^{-2}.)	0.5 M NaOH + 2.0 M CH_3OH	Int. J. Hydrogen Energy 2020, 45, 4444
Pd-PdO PNTs-260	1.11 (A mg^{-1})	1.0 M KOH + 1.0 M CH_3OH	Adv. Funct. Mater. 2020, 2000534
$Au_{80}@Pd_{20}/C$	0.83 (A mg−1 Pd)	0.5 M KOH + 0.5 M CH_3CH_2OH	Appl. Catal. B-Environ. 2019, 251, 313
Au@PdAg-NTs	3.5 (mA cm^{-2}.)	1.0 M KOH + 1.0 M CH_3OH	RSC Adv., 2019, 9, 931
2D/1D Au/Pd	0.62 (A mg−1 Pd)	1.0 M KOH + 1.0 M CH_3CH_2OH	ACS Appl. Mater. Interfaces 2019, 11, 20117
PdNW@cCuO_2	0.57 (A mg−1 Pd)	1.0 M KOH + 1.0 M CH_3OH	Small 2019, 1904964
Au-Pd alloy	2.81 (mA cm−2 Pd.)	1.0 M KOH + 1.0 M CH_3OH	J. Phys. Chem. C 2018, 122, 21718
HOH-shaped $Au@Au_{0.2}Pd_{2.0}$ NPs	11.9 (A mg−1 Pd)	0.5 M KOH + 0.5 M CH_3CH_2OH	J. Mater. Chem. A, 2018, 6, 7675
PdAg NDs	2.6 (A mg−1 Pd)	1.0 M KOH + 1.0 M CH_3CH_2OH	Adv. Mater. 2018, 1706962
Pd_2Au-180	0.49 (A mg−1 Pd)	1.0 M NaOH + 1.0 M CH_3OH	Electrochim. Acta 2018, 259, 284
$Pd_{40}Ni_{43}P_{17}$	4.95 (A mg−1 Pd)	1.0 M NaOH + 1.0 M CH_3CH_2OH	Nat. Commun. 2017, 8, 14136
Au@Pd NRs	2.92 (A mg−1 Pd)	1.0 M KOH + 1.0 M CH_3CH_2OH	Adv. Mater. 2017, 29, 1701331
core–shell Au–Pd nanodendrites	1.2 (A mg−1 Pd)	1.0 M KOH + 0.5 M CH_3CH_2OH	Nanoscale, 2017, 9, 12494
$Pd_{67}Au_{33}/C$	129.85 (mA cm^{-2}.)	0.5 M NaOH + 1.0 M CH_3CH_2OH	J. Power Sources 2017, 361, 276
Pd_1Au_1 porous foam films	0.2723 (mA cm^{-2}.)	0.5 M KOH + 0.5 M CH_3OH	Catal. Commun. 2016, 73, 22

PdCuCo NCs/C-375℃	7.72 (A mg−1 Pd)	1.0 M NaOH + 1.0 M CH_3CH_2OH	Angew. Chem. Int. Ed. 2016, 55, 1
$Pd_{30}Au_{70}$/C	0.95 (A mg−1 Pd)	1.0 M KOH + 1.0 M CH_3OH	J. Mater. Chem. A, 2013, 1, 9157
PdCuSn/CNTs	0.40 (A mg−1 Pd)	1.0 M KOH + 0.5 M CH_3OH	J. Power Sources 2013, 242, 610
NP-PdAu	0.87 (A mg−1 Pd)	0.5 M KOH + 1.0 M CH_3OH	J. Alloy. Compd. 2013, 565, 120
Au@Pd	7.89 (mA cm^{-2}.)	1.0 M KOH + 0.5 M CH_3OH	J. Catal. 2012, 295, 217

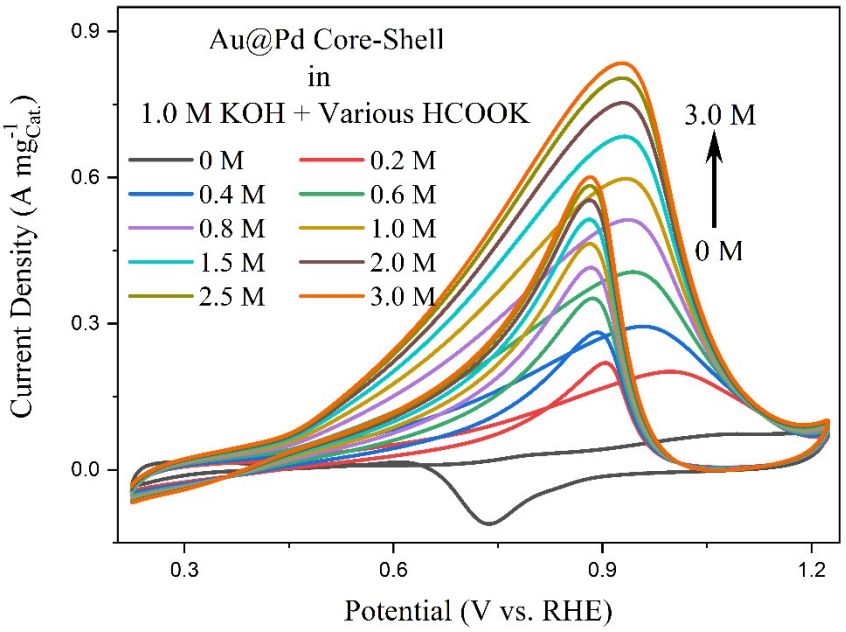

Figure S8 Electrocatalytic activity of formate oxidation on the as-prepared Au@Pd_Core-Shell nanoparticles. The CV curves were recorded in N_2-saturated 1.0 M KOH solution with various HCOOK concentrations. The scan rate was 50 mV s^{-1}.

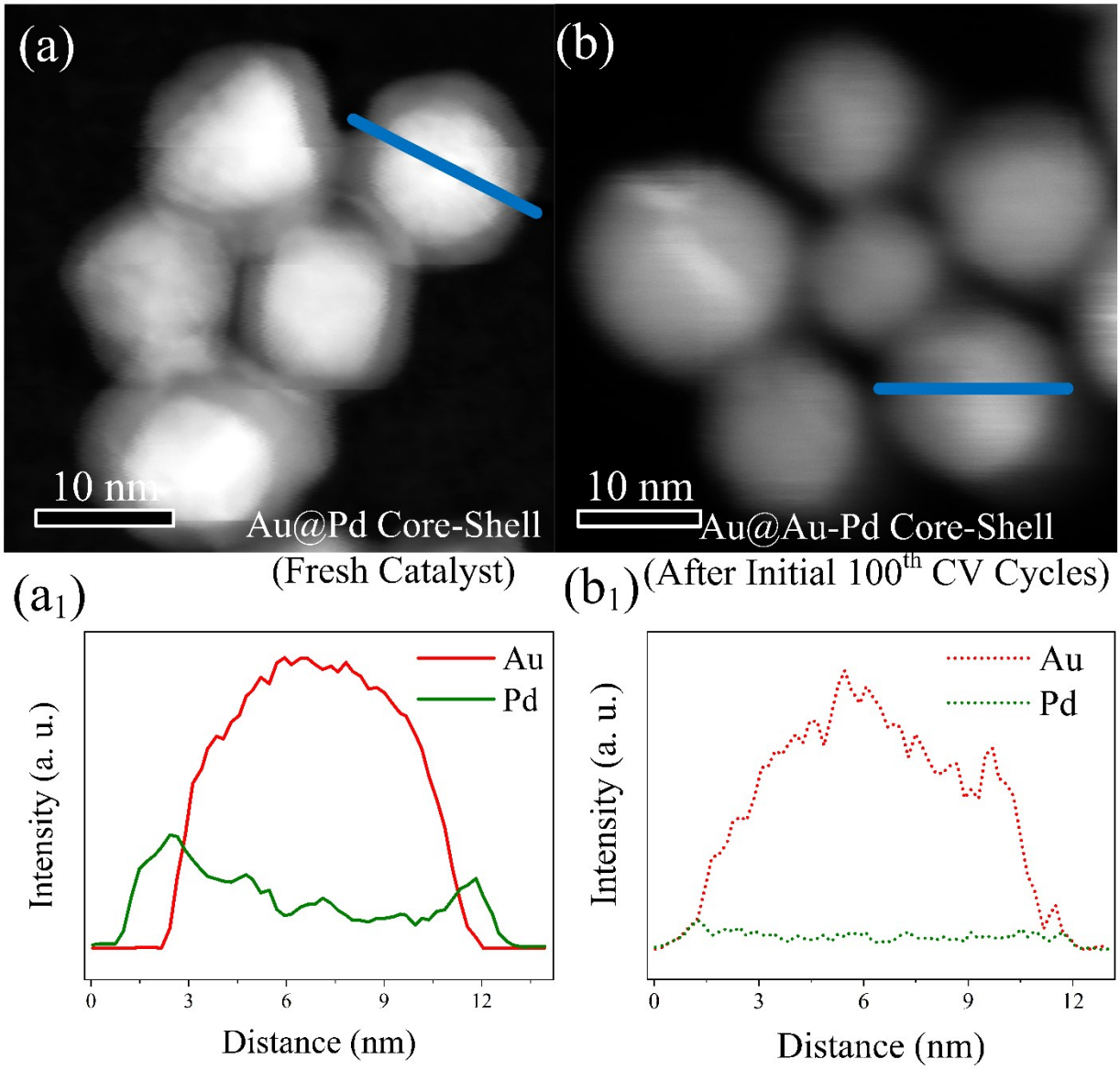

Figure S9 Microstructure characterization of the as-prepared Au@Pd_Core-Shell nanoparticles. HAADF-STEM images of the nanoparticles at (a) before and (b) after the initial 100th successive CV cycling test for MOR. The EDS line scan of individual nanoparticle at (a_1) before and (b_1) after the initial 100th successive CV cycling test for MOR. The initial 100th successive CV cycling test was performed in a N_2-saturated 1.0 M KOH solution with 1.0 M CH_3OH at a scan rate of 50 mV s^{-1}.

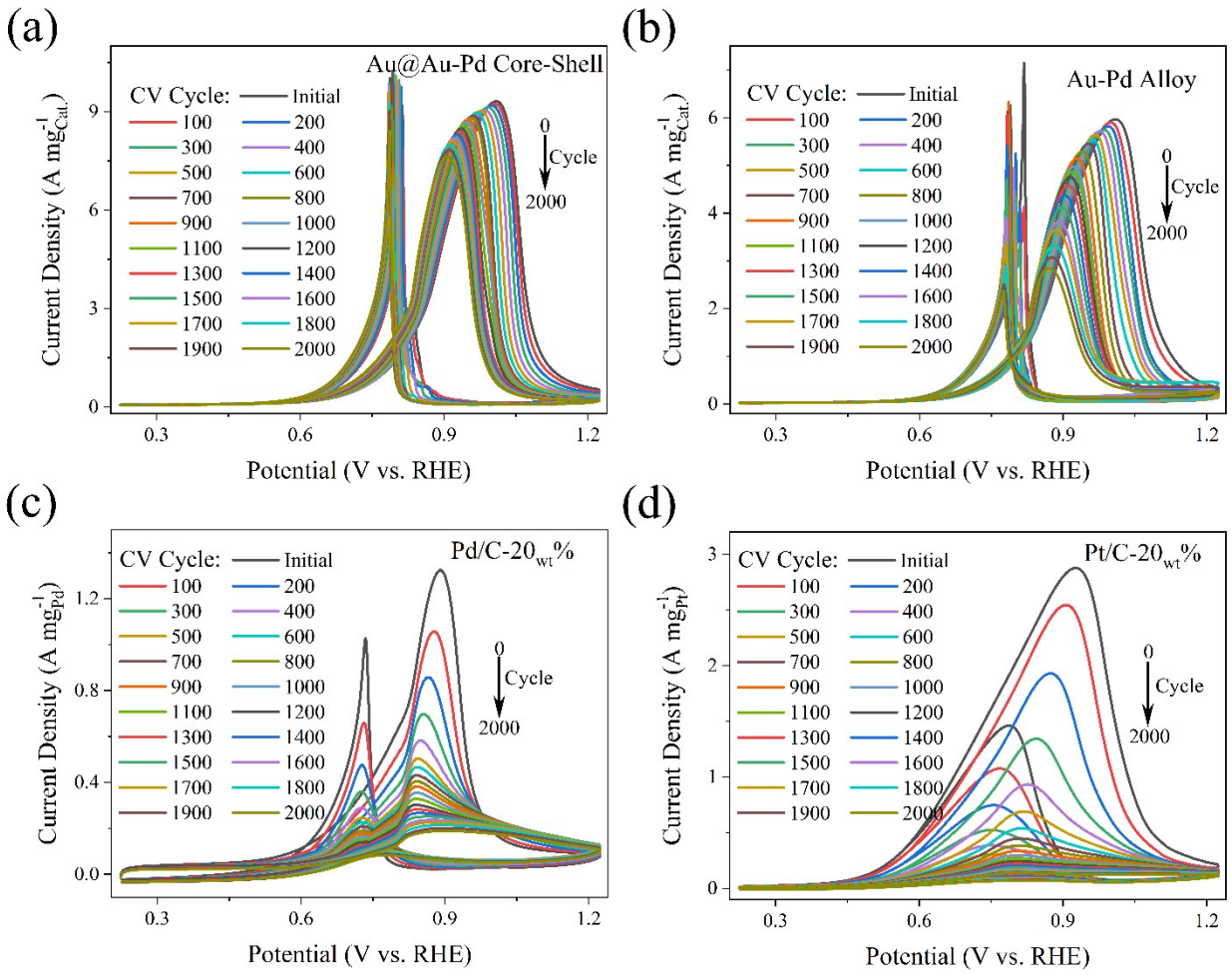

Figure S10 Results of the CST over 2000 CV cycles, collected at 10-scan intervals: (a) as-obtained Au@Au-Pd_Core-Shell, (b) Au-Pd_Alloy, (c) commercial Pd/C-20$_{wt}$%, and (d) commercial Pt/C-20$_{wt}$% catalysts. The CST was performed in an N_2-saturated 1.0 M KOH solution with 1.0 M CH_3OH. The scan rate was 50 mV s^{-1}.

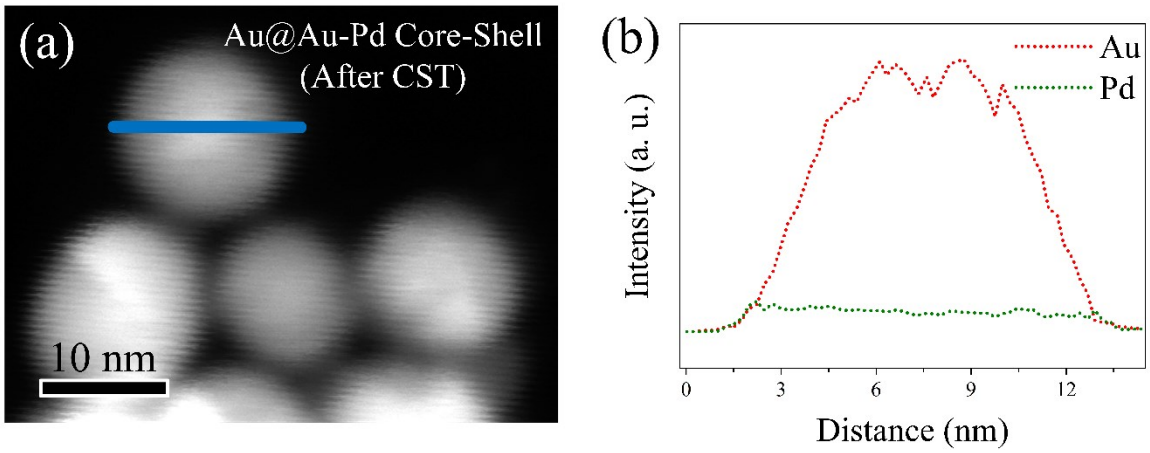

Figure S11 Electrocatalytic effect on the microstructure of the as-obtained Au@Au-Pd_Core-Shell catalyst: HAADF–STEM images of the Au@Au-Pd_Core-Shell nanoparticles (a) before and (a_1) after the CST, and the corresponding EDS line scan of an individual nanoparticle (b) before and (b_1) after the CST.

Table S2 Atomic ratios of the Au and Pd components in the samples.

Sample / Counts (%)	Au@Pd_Core-Shell	Au-Pd_Alloy	Au@Au-Pd_Core-Shell	Au@Au-Pd_Core-Shell (After CST)
Pd	28.44	51.13	18.45	18.01
Au	71.56	48.87	81.55	81.99

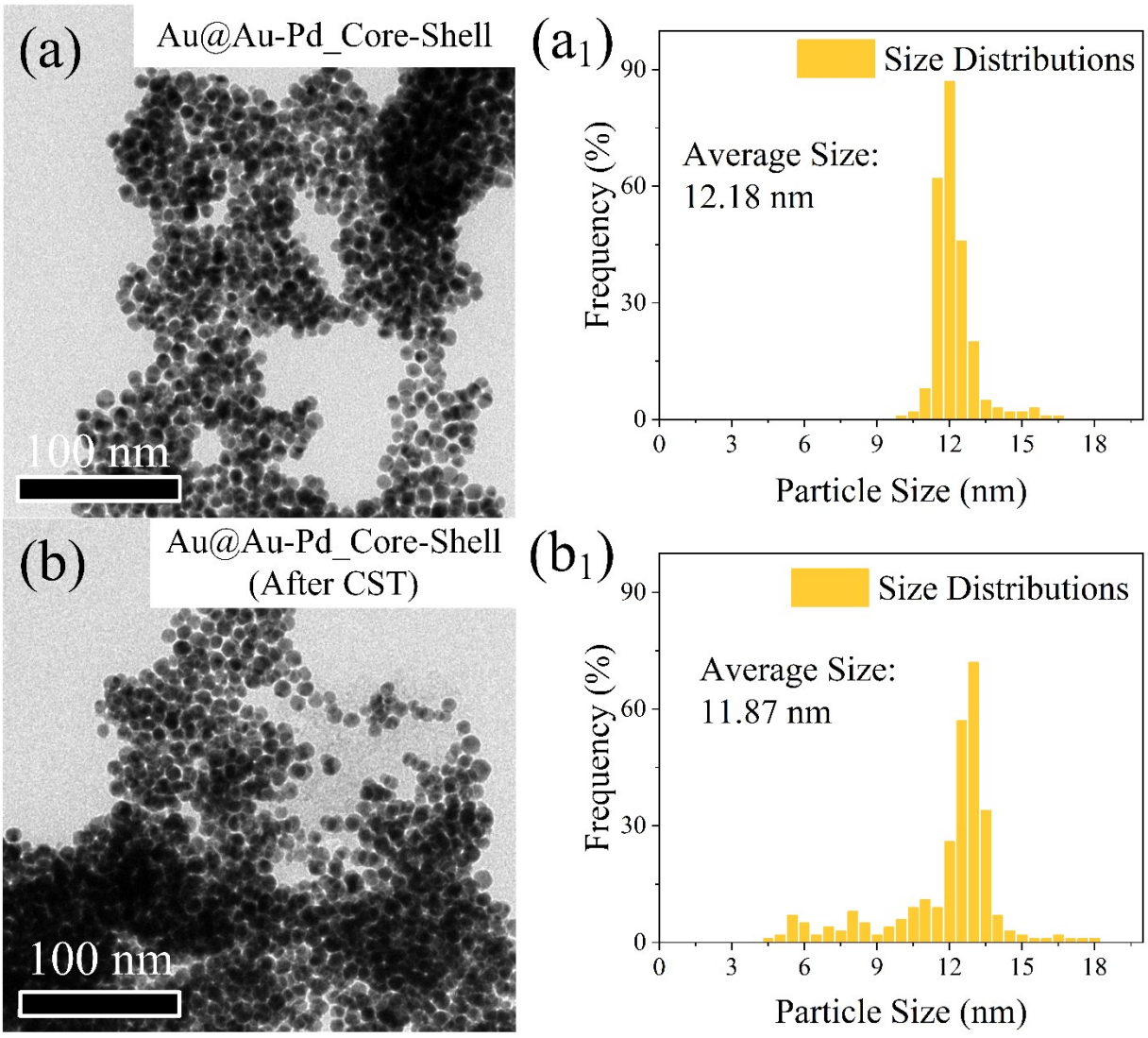

Figure S12 (a-b) Bright field TEM images and corresponding nanoparticle size distributions of the as-obtained Au@Au-Pd_Core-Shell before (a, a_1) and after (b, b_1) the cycling stability test (CST).

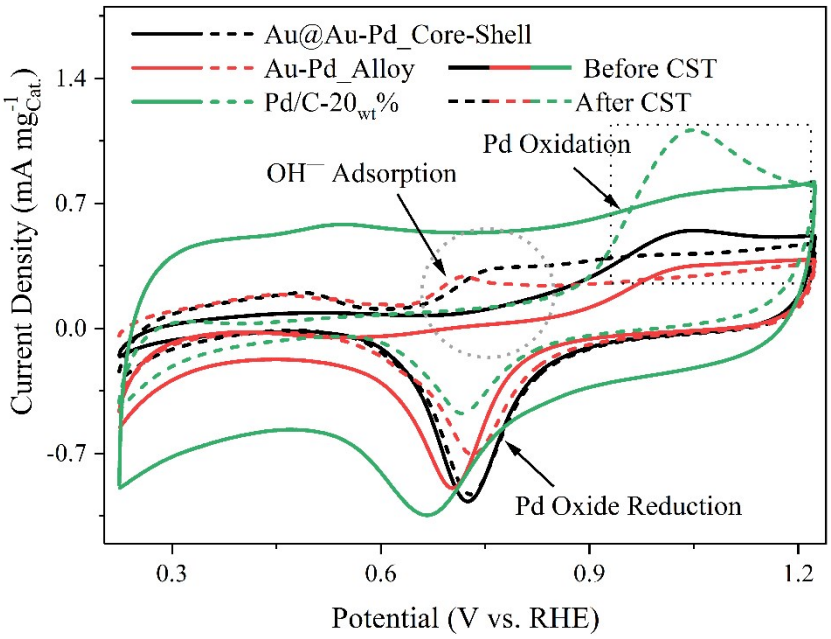

Figure S13 Electrochemical performances of the as-obtained Au@Au-Pd_Core-Shell, Au–Pd_Alloy, and commercial Pd/C-20$_{wt}$% catalysts before and after the CST. The CV curves were recorded in N_2-saturated 1.0 M KOH solution. The scan rate was 50 mV s^{-1}.

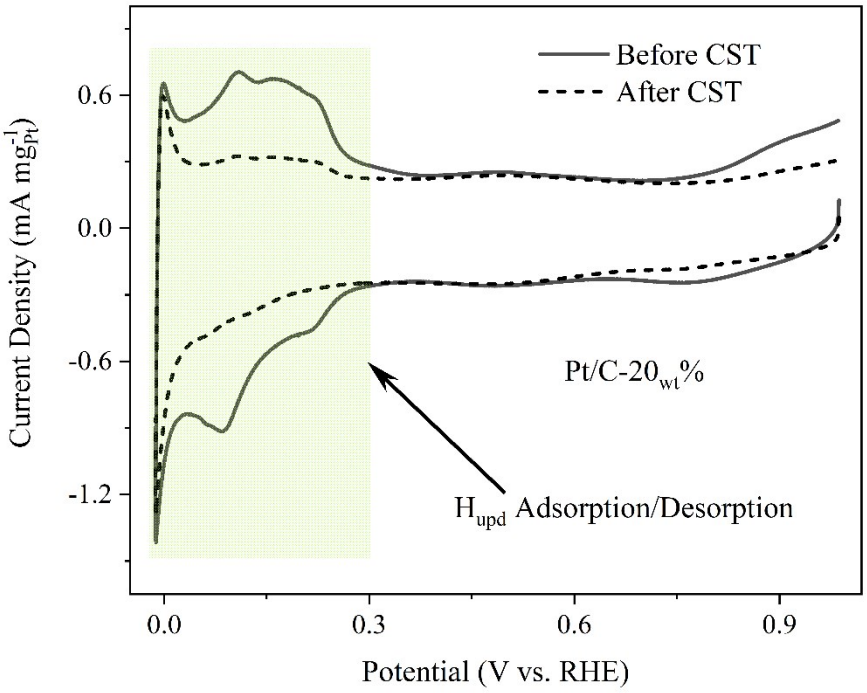

Figure S14 CV curve of the commercial Pt/C-20_{wt}% catalyst in N_2-saturated 0.5 M H_2SO_4 solution before and after CST. The scan rate was 50 mV s^{-1}.

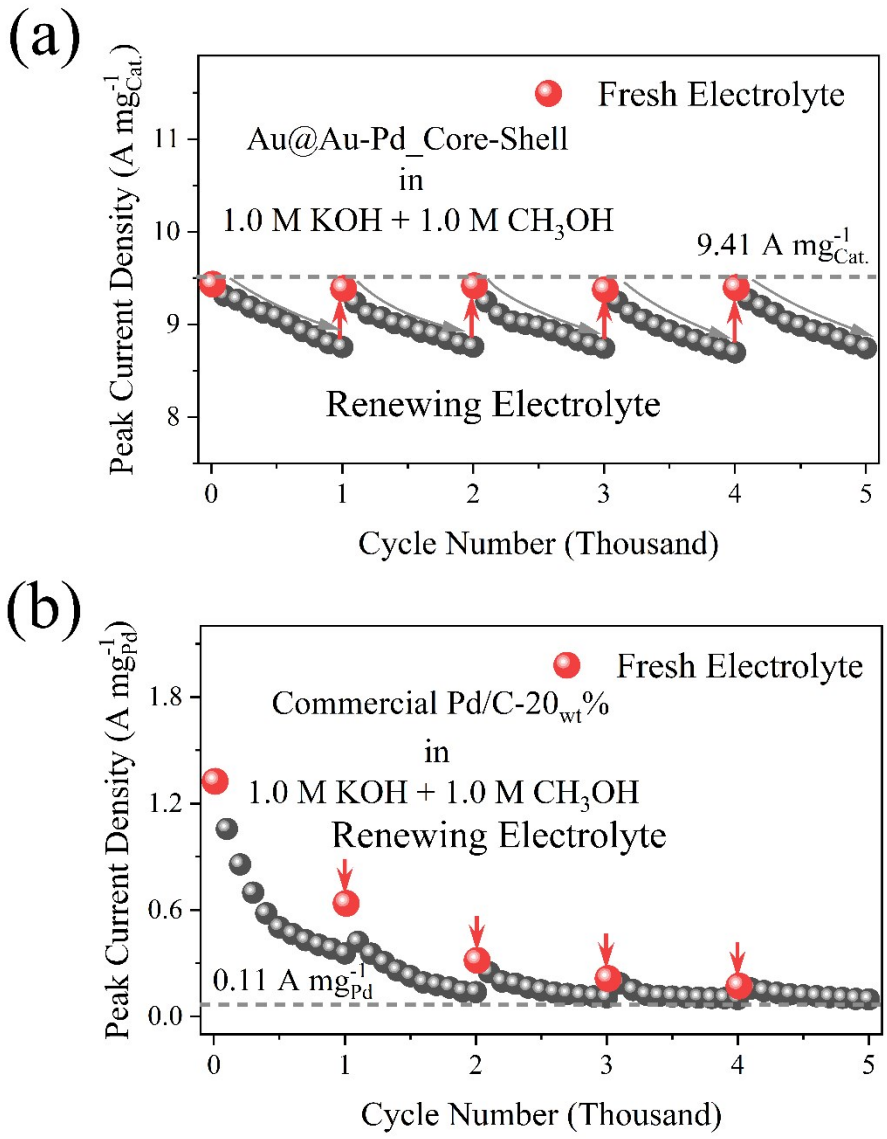

Figure S15 Plots of MOR anodic peak current mass density versus cycle number in the (a) as-obtained Au@Au-Pd_Core-Shell and (b) commercial Pd/C-20$_{wt}$% catalysts. The electrolyte was refreshed at intervals of 100 CV cycles.

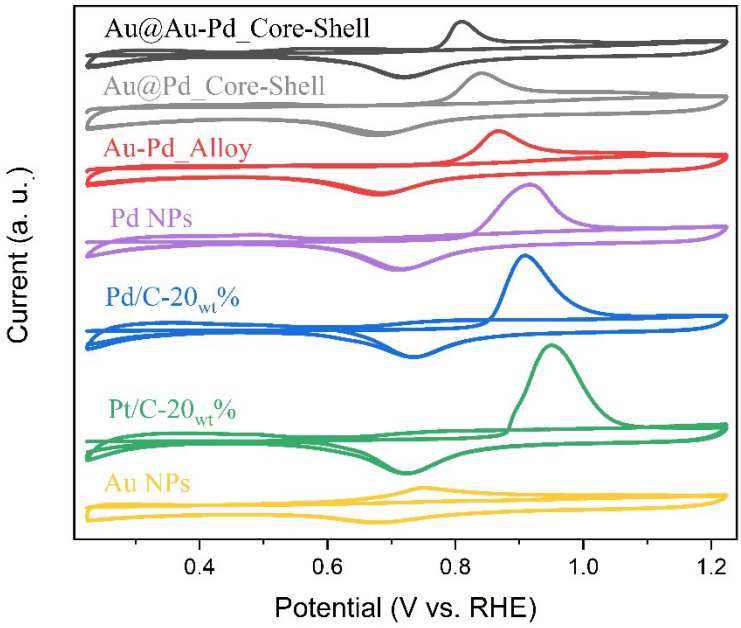

Figure S16 CO-Stripping curves of the as-prepared Au@Pd_Core-Shell, as-obtained Au@Au–Pd_Core-Shell, Au–Pd_Alloy, Pd nanoparticles, Au nanoparticles, Pd/C-20_{wt}%, and Pt/C-20_{wt}%.